PERSPECTIVE / REVIEW

Circumferential Coloration of Image Fibers on the Shroud of Turin

Evidence, Physical Constraints, Hypothesized Mechanisms, and Decisive Tests

Otangelo Grasso

Independent Researcher — Aracaju, SE, Brazil

otangelograsso@gmail.com · ORCID 0009-0005-6942-0593

August 2026

Written with the support and assistance of AI tools.

Contents

Abstract 1

1. Introduction 2

PART I — THE EVIDENCE 3

2. "Superficiality" Is Not One Observation 3

2.1 Cloth-level superficiality 3

2.2 Thread-level superficiality 3

2.3 Individual-fiber superficiality 4

3. The Evidentiary Status of the 360° Claim 4

3.1 What the early STURP literature established 4

3.2 Development of the explicit circumferential formulation 5

3.3 Evidentiary ranking 5

4. The Longitudinal Discontinuity Problem 5

5. What Material Is Actually Colored? 6

5.1 Structural polysaccharide alteration 6

5.2 Primary cell wall (Fanti) 6

5.3 External carbohydrate coating (Rogers) 7

5.4 Pectin (Jaworski) 7

6. The Combined Microscopic Constraint 7

PART II — HYPOTHESIZED EXPLANATIONS 10

7. Directional UV and Vacuum-UV Radiation 10

8. Directional Photons: The Absorption, Transmission, and Chemical-Response Problem 11

8.1 Homogeneous absorber: the classical contradiction 11

8.2 Two-layer optical transfer: absorption contrast helps, but does not by itself equalize both sides 11

8.3 The viable optical escape: combine transfer with a nonlinear chemical response 12

9. Gas-Phase Maillard Reaction 13

10. Substrate Selectivity: Why Chemical Response ≠ Deposited Energy 13

11. Corona Discharge and Electrical Surface Processes 14

12. Rucker's Two-Stage Radiation/Electrical Model 15

12.1 The classical skin-effect implementation is not established for flax 15

13. A Distinct Gamma/Secondary-Electron Mechanism 16

13.1 Coupling of the two nuclear channels 16

14. The Selectivity-versus-Uniformity Problem, Quantified 17

15. A Surface-Propagation Hypothesis 18

PART III — DECISIVE EXPERIMENTS 18

16. Experiment 1 (Priority): Establish Whether the 360° Shell Exists 19

17. Experiment 2: Quantify Circumferential Completeness 19

18. Experiment 3: Joint Optical-Transfer and Chemical-Response Test of Directional VUV 19

19. Experiment 4: Test Gas/Coating Selectivity at Fiber Resolution 20

20. Experiment 5: Revisit Corona Discharge Without Thermal Confounds 20

21. Experiment 6: Quantitatively Test the Skin-Effect Proposal 20

22. Experiment 7: Microdosimetry Test of the Gamma/Secondary-Electron Model 21

23. Comparative Assessment 21

PART IV — DISCUSSION 22

24. The Central Paradox Is a Change of Symmetry 23

25. What Would Most Strongly Discriminate the Models 24

26. A Necessary Terminological Correction 25

27. Implications if the 360° Shell Is Confirmed 25

28. Implications if the 360° Shell Is Not Confirmed 25

29. Limitations and Critical Perspectives 29

29.1 Source concentration and independence 29

29.2 A convergence that should raise suspicion, not confidence 30

29.3 The radiocarbon date deserves primary, not incidental, treatment 30

30. Conclusion 31

Source-Critical and Methodological Note 32

AI-Assistance Disclosure 32

Conflict of Interest 33

References 33

Abstract

Among the microscopic characteristics attributed to the body image on the Shroud of Turin, one of the most physically restrictive is the reported circumferential coloration of individual image fibers. The body image is demonstrably superficial at the cloth and thread levels. Later microscopy further indicates that the alteration on some extracted image fibers is confined to an external submicrometer region, associated by Fanti and co-workers with the primary cell wall, and may extend around the cylindrical fiber surface. These observations are often bundled together as though they possess equal evidentiary weight; they do not.

This paper therefore proceeds evidence first. STURP-era work securely established cloth- and thread-level superficiality, lack of liquid capillarity, preferential coloration of exposed thread crowns, and chemical alteration of image fibrils rather than sufficient applied pigment to account for the body image. The stronger individual-fiber proposition—a nearly complete 360° altered shell only a few tenths of a micrometer thick—is principally grounded in later microscopy. Fanti et al. reported a direct optical estimate of approximately 0.2 ± 0.2 μm at a lacuna in the outer layer of a tape-extracted Shroud image fiber, while also arguing that the colored exterior could be observed from opposite sides. This is substantive evidence, but it is neither a modern nanoscale chemical tomography nor evidence that every image fiber has an identical shell.

Granting the strong circumferential interpretation provisionally, candidate mechanisms are then evaluated against the combined microscopic constraints: radial superficiality, thread-crown preference, neighboring colored and clear fibers, abrupt longitudinal termination, possible circumferential completeness, and macroscopic image encoding. Directional UV/VUV irradiation is experimentally strong for superficial photochemistry but, if a complete shell is real, requires a joint optical-and-chemical explanation of near-side, interior, and far-side responses. A Rogers-type Maillard reaction acting in a surface carbohydrate layer naturally permits circumferential access and superficial chemistry but struggles with microscopic selectivity and sharp switching. Corona/electrical mechanisms permit threshold and circumferential behavior but remain experimentally incomplete. Rucker's current radiation/electrical model is correctly separated from a distinct gamma/secondary-electron proposal: his January 2026 mechanism invokes proton-driven alternating current and classical skin effect, whereas the latter relies on photon transport and secondary-electron microdosimetry. Under ordinary cellulose dielectric behavior, the classical good-conductor skin-effect approximation is not applicable; a viable version would require a transient conductive state that has not been quantitatively specified or demonstrated.

A further result concerns stochastic explanations of fiber selectivity. Under an explicit independent-event model in which otherwise comparable neighboring fibers differ mainly because of Poisson fluctuations, rare-event selectivity and a smoothly complete circumferential

shell impose opposing event-density requirements unless one trigger produces a much larger circumferential response. This does not prove that propagation is universal, because fiber-to-fiber chemical heterogeneity could also create selectivity; it does show that independent local hits alone are insufficient under the stated assumptions. The highest-priority next step is therefore empirical: modern three-dimensional chemical mapping of authenticated image fibers as a function of radial depth r, circumferential angle θ, and longitudinal position z. If a continuous ultrathin 360° shell is confirmed, it will impose a severe and highly discriminating boundary condition. If not, a major objection to directional mechanisms substantially weakens.

Keywords: Shroud of Turin; flax fiber; image formation; superficiality; primary cell wall; circumferential coloration; STURP; vacuum ultraviolet; corona discharge; Maillard reaction; radiation transport; microdosimetry.

1. Introduction

The Shroud of Turin bears faint frontal and dorsal body images on linen woven from flax. The mechanism responsible for the body image remains unresolved. During the 1978 Shroud of Turin Research Project (STURP), the cloth was examined by optical, spectroscopic, chemical, photographic, microscopic, radiographic, and related methods. The principal STURP chemical and physical syntheses concluded that the body image could not be accounted for by an applied quantity of pigment, dye, or stain sufficient to form the image and that image coloration involved chemical alteration of the linen fibrils, commonly described in terms of oxidation and dehydration of carbohydrate material [1–3]. Walter McCrone disputed this interpretation and argued for an artist-pigment model; that disagreement is a useful reminder that observations and interpretations must be kept distinct.

One characteristic has acquired exceptional importance in image-formation discussions: circumferential coloration of individual image fibers. In its strongest modern formulation, a flax fiber roughly 10–20 μm in diameter has an essentially uncolored interior while an external submicrometer layer is yellowed around much or all of its cylindrical circumference. Fanti et al. described this interpretation explicitly and associated the altered region with the primary cell wall [6].

If correct in the strong form, this is an extraordinary boundary condition: a mechanism must be directionally selective at the scale of the cloth while becoming approximately azimuthally nondirectional at the scale of a single fiber. A vertically incident agent encounters the body-facing side of a fiber before its interior and far surface; if the agent directly causes chemical modification, straightforward directional exposure predicts stronger alteration on the incident hemisphere. Yet the microscopy literature describes an altered region extending around the cylindrical surface.

The problem is more demanding because circumferentiality is not the only microscopic constraint. Coloration occurs preferentially on exposed portions of threads; nearby fibers can differ markedly in coloration; and individual colored segments can terminate sharply along a fiber's length. Moran and Fanti illustrated tape-extracted image fibers with abrupt longitudinal boundaries across approximately the full fiber diameter [7]. That observation concerns the ends of colored segments, not a boundary between the illuminated and non-illuminated hemispheres of a cylindrical fiber; it therefore adds a constraint rather than contradicting circumferential coloration.

A successful mechanism must therefore explain how a coloration event could simultaneously be (1) superficial through the cloth; (2) concentrated near exposed thread crowns; (3) selective among neighboring fibers; (4) capable of abrupt longitudinal termination; (5) confined to an ultrathin radial region; (6) potentially circumferential within that region; and (7) spatially organized across millions of fibers into a coherent image.

This paper separates evidence from explanation. Sections 2–6 establish what is directly supported, what is inferred, and how strongly each claim should be weighted. Sections 7–15 then examine hypothesized mechanisms. Sections 16–22 propose discriminating experiments. The aim is deliberately narrow: to determine what physical processes could or could not reproduce the reported microscopic structure, without adjudicating the historical identity of the cloth or inferring a theological event from the microscopy.

PART I — THE EVIDENCE

2. "Superficiality" Is Not One Observation

Image superficiality is used as though it named a single phenomenon; at least three distinct scales are involved.

2.1 Cloth-level superficiality

STURP-era work established that the body image is associated principally with the cloth surfaces rather than penetrating the full fabric thickness. Schwalbe and Rogers emphasized the absence of liquid capillary behavior and the concentration of image coloration on exposed parts of the weave, and concluded that an oxidation–dehydration process affecting the linen fit the data better than an applied pigment, while stating explicitly that the transfer mechanism remained unknown. Strong observation.

2.2 Thread-level superficiality

Microscopy showed preferential coloration on fibers near thread crowns — the portions most geometrically exposed — with only the uppermost fiber layers significantly affected rather than the whole bundle. Strongly supported. It follows that any freely penetrating liquid is immediately problematic, since a liquid entering by capillarity follows interfiber spaces rather than halting at the upper few fibers.

2.3 Individual-fiber superficiality

The strongest formulation concerns the fiber itself: the visible alteration is interpreted as confined to a very thin outer region while the interior remains substantially colorless. Fanti and co-workers examined STURP adhesive-tape fibers and described both circumferential surface coloration and a lacuna in the colored exterior of a Shroud image fiber through which brighter, colorless internal material could be seen. At that lacuna they estimated the thickness of the primary-cell-wall region as approximately 0.2 ± 0.2 μm [6].

That value must be handled carefully. It is a direct optical estimate on tape-extracted Shroud material, not merely a value imported from an experimental VUV replica; however, its uncertainty is of the same order as its central value, the primary cell wall is not expected to have perfectly uniform thickness, and no modern nanoscale cross-sectional chemical survey has established that the same thickness applies around the full circumference of many independent image fibers. The defensible formulation is therefore that the image alteration has been reported in an external submicrometer region, plausibly of primary-cell-wall scale and on the order of a few tenths of a micrometer—not that every image fiber is colored to a precisely measured 0.200 μm depth.

3. The Evidentiary Status of the 360° Claim

3.1 What the early STURP literature established

The STURP literature discusses superficial fibril coloration, image-fiber chemistry, thread-crown effects, and the halftone character of image density. Adler emphasized that individual image fibers tend to possess comparable coloration and that macroscopic image intensity is controlled substantially by the fraction of colored fibers rather than by large changes in individual-fiber darkness. His exact statement is worth quoting, because it is frequently over-read:

> *"All the colored fibers are uniformly colored, i.e., an exposed fiber is either colored or not colored. This demonstrates that the image seen at the macroscopic level is an areal density image and not a pigment concentration image." (Adler, 1999)*

Adler's "uniformly colored" thus means colored-versus-uncolored — an areal-density (halftone) argument — not a statement about azimuthal completeness around a single fiber. In the same

passage he describes the image as going "only one fiber deep lying on top of the crowns of the threads," with no 0.2 μm figure and no 360° claim. Translating Adler into "STURP measured a complete 360° shell around every image fiber" is therefore an over-reading of the primary source.

3.2 Development of the explicit circumferential formulation

The explicit proposition that a colored fiber is uniformly colored around its cylindrical surface appears in the Shroud Science Group evidence catalogue presented at the Third Dallas International Conference in 2005 [5]. The catalogue cites Adler (1996, 1999) for the proposition. The strongest direct observational argument, however, is Fanti et al. (2010): extracted image fibers were reported to remain colored when viewed from opposite sides in reflected-light microscopy, while broken or missing exterior regions exposed brighter, uncolored internal material [6]. This is substantive evidence for a circumferential external alteration, but the method remains optical microscopy of tape-extracted fibers rather than nanoscale three-dimensional chemical tomography.

3.3 Evidentiary ranking

High confidence: body-image coloration is highly superficial at fabric scale; exposed thread surfaces are preferentially involved; liquid-like capillary penetration is absent; image and background fibers differ chemically/optically; interiors of examined image fibers appear substantially less colored than their superficial regions; neighboring colored and clear fibers occur; and abrupt longitudinal color terminations have been reported [1–7].

Moderate confidence: image-related alteration is confined to an external submicrometer region of at least some individual image fibers, and that region is broadly compatible with primary-cell-wall dimensions [6].

Important but insufficiently quantified: essentially complete 360° coverage on most or all image fibers; equal chemical intensity on the near and far hemispheres; uniform shell thickness around the circumference; and universality of this morphology across different image regions and image intensities.

The circumferential observation should therefore be neither dismissed nor elevated beyond what has been measured.

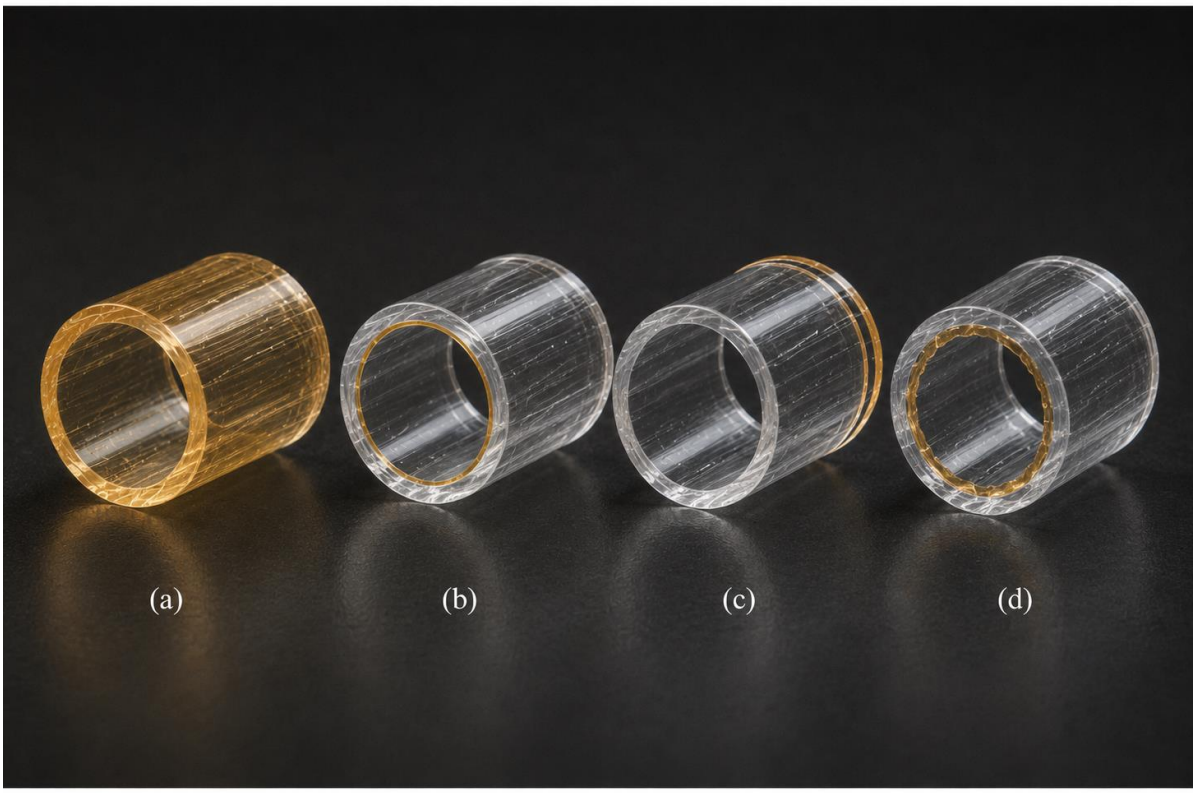
4. The Longitudinal Discontinuity Problem

Moran and Fanti reported tape-extracted image fibers with sharp boundaries between colored and uncolored longitudinal segments, describing boundaries across roughly the ~15 μm fiber diameter rather than a long gradual transition [7]. This is potentially diagnostic, but the samples were collected by adhesive tape and mechanically stressed; therefore the morphology should be re-

examined with modern imaging before its transition length is treated as a precise intrinsic material constant. If confirmed, however, a switch-like longitudinal boundary favors either a very steep exposure gradient, a nonlinear chemical threshold, or a secondary activation process over simple unconstrained diffusion.

5. What Material Is Actually Colored?

Figure 4 — Four Candidate Substrates



Illustrative renderings of four candidate substrate hypotheses — not photomicrographs of Shroud material.

Figure 4. Four candidate substrate hypotheses for the altered layer, compared at the same scale (§5). (a) whole structural-polysaccharide alteration; (b) primary cell wall only (Fanti); (c) an external carbohydrate coating, physically distinct from the fiber wall (Rogers); (d) a thin, irregular pectin-rich sublayer within the primary cell wall (Jaworski). Illustrative rendering, not a photomicrograph of Shroud material.

Even with the altered layer's geometry known, its chemical substrate is uncertain, and the mechanism analysis depends on which substrate holds. We therefore treat the mechanism sections (7–15) as conditional on substrate identity, which is itself an open experimental question (Section 16).

5.1 Structural polysaccharide alteration

Heller and Adler's microchemistry supported dehydration and oxidation of polysaccharide material, producing conjugated chromophores; the ACS STURP synthesis likewise concluded the image involved chemical modification rather than sufficient applied pigment.

5.2 Primary cell wall (Fanti)

Fanti and co-workers interpret the colored region as the flax primary cell wall — geometrically attractive because the PCW forms a thin outer envelope. If the reactive substrate is already an external cylindrical shell, circumferential coloration becomes less surprising: the mechanism need only activate a substrate that is circumferential by construction.

5.3 External carbohydrate coating (Rogers)

Rogers proposed a different substrate: ancient linen preparation could leave starch fractions, reducing saccharides, and Saponaria residues concentrated at evaporating surfaces, with volatile amines from decomposition driving amino-carbonyl (Maillard) reactions in this thin external impurity layer rather than in structural cellulose. This removes a standard objection to gaseous mechanisms: a gas may permeate the spaces around a fiber while the reactive substrate remains external, so the reaction need not penetrate.

We note explicitly that adopting Rogers's substrate while not adopting his rejection of radiation/corona mechanisms is a deliberate decoupling — and a legitimate one, because the substrate claim (where the reactive material sits) and the mechanism claim (what activates it) are logically independent.

5.4 Pectin (Jaworski)

Jaworski emphasizes pectins in the primary cell wall — chemically less resistant than crystalline secondary-wall cellulose and thus a selectively vulnerable outer substrate. His FTIR analysis does not positively demonstrate surviving pectin in image fibers; it argues the spectra do not exclude its former presence and that pectic material could have been preferentially destroyed during image formation.

Consequently: the geometry of the altered layer and its chemistry must not be conflated. PCW cellulose, hemicellulose/pectin, and an external manufacturing-derived coating lead to different predictions for any proposed mechanism, and each mechanism below is assessed noting which substrate it requires.

6. The Combined Microscopic Constraint

Let $C(r, \theta, z)$ denote the degree of image-related chemical alteration in a fiber, with r radial depth, θ circumferential angle, z longitudinal position. The strong interpretation requires $C > C_{th}$ within

an ultrathin shell $R - t < r < R$ for most or all $0 \le \theta < 2\pi$, while $C \approx 0$ in the interior. Simultaneously, for some neighbor fiber j, $C_j \approx 0$, and along a colored fiber C can fall to background across a short distance in z. The mechanism must therefore generate, in one process:

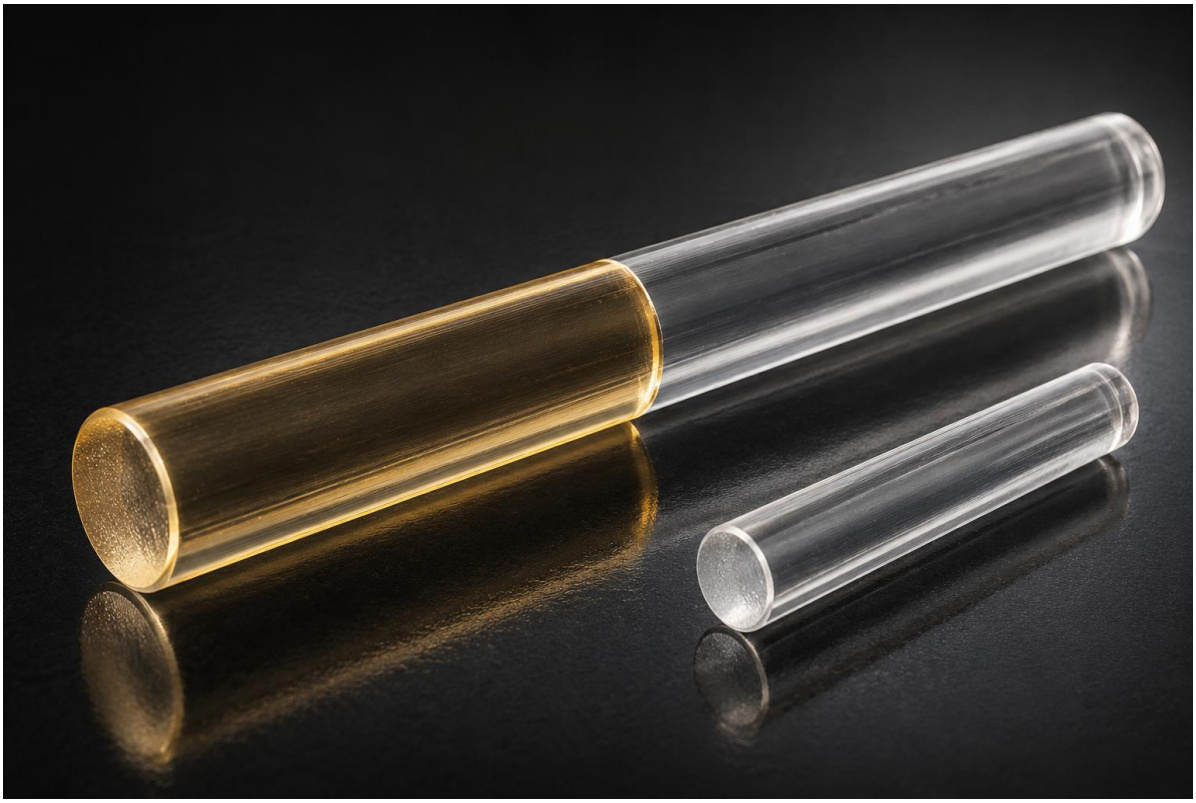


Figure 3. The C(r, θ, z) constraint space (§6). A single fiber's altered outer shell (gold) terminates abruptly along the fiber's length (z), transitioning to unaltered material beyond that point — the "longitudinal switching" constraint. A neighboring fiber (foreground) shows no alteration at all, illustrating the "neighbor selectivity" constraint. Radial (r) and circumferential (θ) structure are represented by the shell's confinement to a thin outer layer running the full circumference. Illustrative rendering, not a photomicrograph of Shroud material.

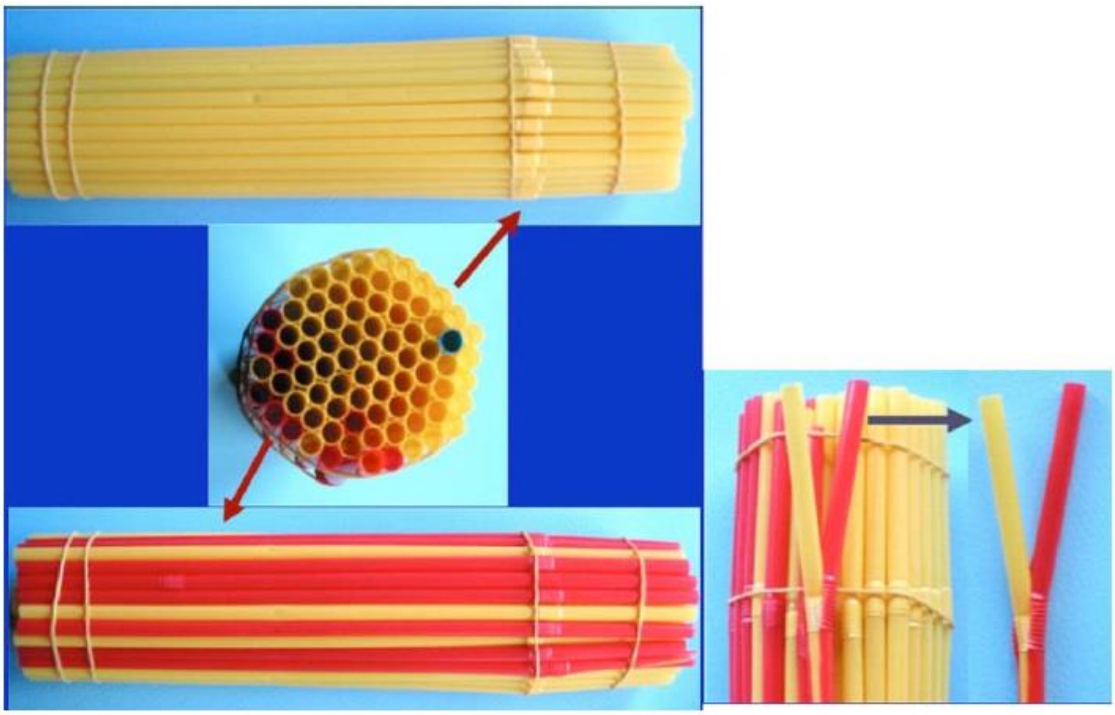


Figure 6 (Fanti). Not a photomicrograph but the original source author's own conceptual macromodel (§6): a Shroud thread represented as a bundle of drinking straws. Top left: a non-image thread, uniformly uncolored. Bottom left: an image thread, with colored (red) straws interspersed among uncolored (yellow) ones — a physical analogy for neighbor selectivity. Right: a single colored straw, showing color confined to its surface with a clear interior — the same radial-superficiality relationship illustrated schematically in Figure 3. Source: Fanti et al. (2010), Figure 6 [6]. © G. Fanti; reproduced here for research/draft purposes — permission to be confirmed before publication.

- **Radial selectivity:** the chemical response in the outer shell greatly exceeds that in the interior (a response constraint, not directly a dose constraint — see Section 10).
- **Circumferential uniformity:** the response is approximately θ-independent within the shell.
- **Neighbor selectivity:** response in a target fiber greatly exceeds that in some adjacent fiber.
- **Longitudinal switching:** $|\partial(\text{response})/\partial z|$ occasionally becomes very large.

This conjunction — not any single feature — is what makes the phenomenon unusual, and it is the standard against which mechanisms are judged below.

PART II — HYPOTHESIZED EXPLANATIONS

7. Directional UV and Vacuum-UV Radiation

The ENEA group (Di Lazzaro and colleagues) used excimer-laser radiation, particularly 193 nm vacuum-ultraviolet, on linen, obtaining very superficial Shroud-like yellowing within a restricted parameter range, with latent coloration developing after aging, and without conventional thermal scorching. This establishes experimentally that high-energy UV photons can produce linen chemistry resembling important aspects of the image. A photochemical model cannot, therefore, be dismissed on the ground that superficial yellowing of flax is impossible; it is demonstrably possible. The authors state explicitly that their process reproduced many, not all, Shroud characteristics, and they did not demonstrate a continuous, uniformly thick circumferential nanolayer. The circumferential requirement is where directional UV meets its central difficulty — analyzed in Section 8, because the usual form of that objection is wrong.

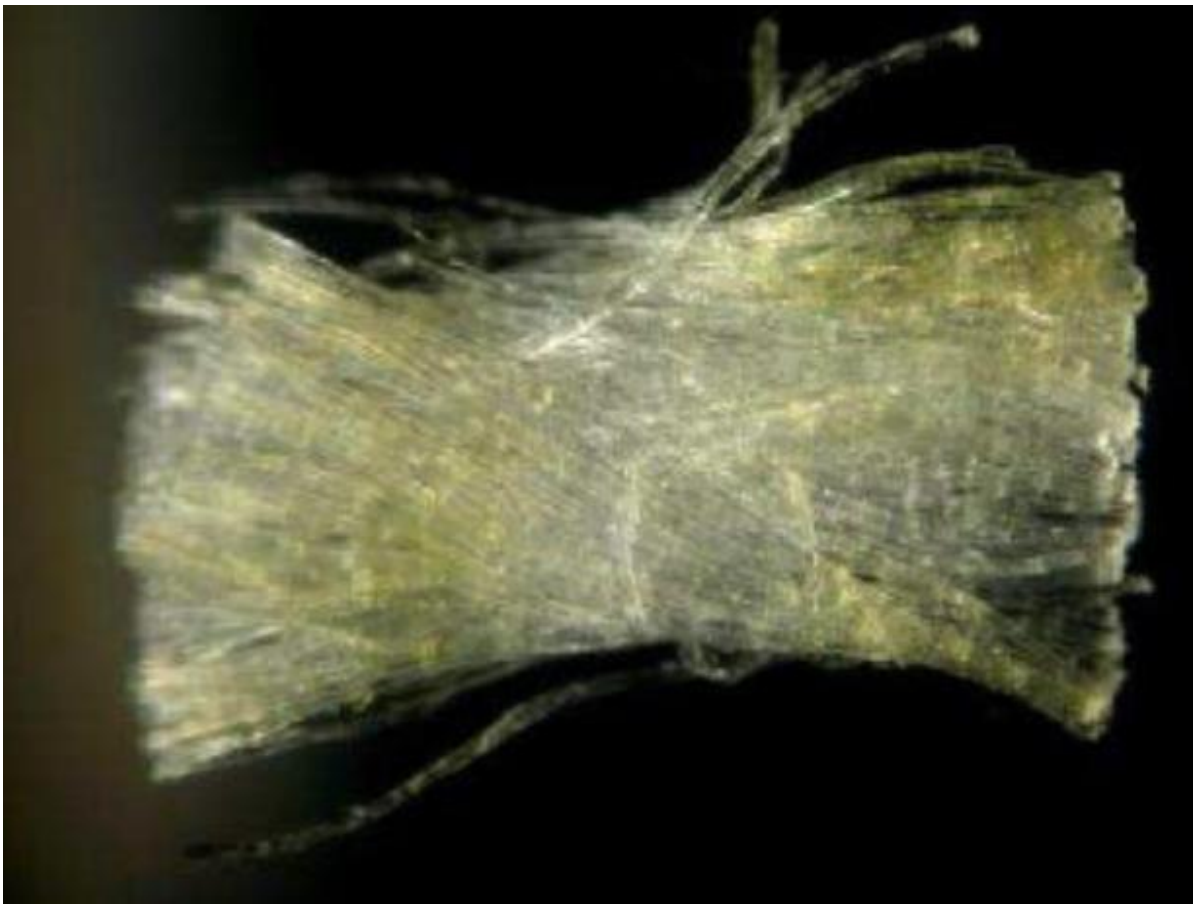


Figure 3b. Real photomicrograph (not a rendering): a linen warp thread after laser irradiation in the vacuum ultraviolet (193 nm), from the ENEA group's replica experiments (§7). The lighter band across the middle is a region shadowed from the beam by an overlying weft thread; individual colored fibers are visible within the thread

bundle, running lengthwise. Source: Di Lazzaro & Murra, "A Ray of Light on the Shroud of Turin" [12]. © the authors; reproduced here for research/draft purposes — permission to be confirmed before publication.

8. Directional Photons: The Absorption, Transmission, and Chemical-Response Problem

A common objection to directional photon models states that radiation capable of producing an ultrathin near-surface reaction cannot also reach the far side of a ~15 μm fiber. That objection is correct for a homogeneous absorber if superficiality is caused by optical attenuation alone. It becomes incomplete, however, when the outer wall and interior differ chemically and optically. The correct question is not simply whether "flax is transparent," but whether the combined optical transfer and composition-dependent photochemical response can produce similar visible alteration in the near and far external layers while leaving the interior below the coloration threshold.

8.1 Homogeneous absorber: the classical contradiction

For incident intensity I_0 in a homogeneous material, Beer–Lambert attenuation gives $I(x) = I_0 \exp(-\alpha x)$. If the relevant attenuation length is only ~0.2 μm, then $\alpha d \approx 75$ for a 15 μm fiber, and the transmitted fraction at the opposite side is $\exp(-75)$, effectively zero. Thus a one-material model in which the same absorption process both confines the reaction and provides the far-side exposure cannot simultaneously produce an ultrathin near-side reaction and comparable direct far-side irradiation.

$$\alpha d \approx d/t \approx 15\ \mu m / 0.2\ \mu m \approx 75.$$

The homogeneous model therefore provides a genuine limiting case, but it is not sufficient to judge substrate models in which the outer primary wall, pectic matrix, or carbohydrate impurity layer differs strongly from the secondary wall.

8.2 Two-layer optical transfer: absorption contrast helps, but does not by itself equalize both sides

Let the near and far external shells each have thickness t and absorption coefficient α_s, while the interior of thickness $d - 2t$ has coefficient α_i. Define optical depths $\tau_s = \alpha_s t$ and $\tau_i = \alpha_i(d - 2t)$. Ignoring reflections for clarity, the energy absorbed in the near shell is proportional to $A_{near} = I_0(1 - \exp(-\tau_s))$, whereas the far-shell absorption is $A_{far} = I_0 \exp(-(\tau_s+\tau_i))(1 - \exp(-\tau_s))$. Consequently, for otherwise identical shells,

$$A_{far} / A_{near} = \exp[-(\tau_s + \tau_i)].$$

This relation is important. A large shell/interior absorption contrast can keep the interior optically transparent while allowing the far shell to receive radiation; however, contrast alone cannot make

far- and near-shell absorbed energies equal if the near shell itself is strongly absorbing. If $\tau_s = 1$ and $\tau_i \ll 1$, for example, the far shell receives only about 37% of the near-shell absorbed energy. Thus the earlier claim that $\kappa = \alpha_s/\alpha_i \gtrsim d/t$ is by itself sufficient for a uniform 360° shell is too strong.

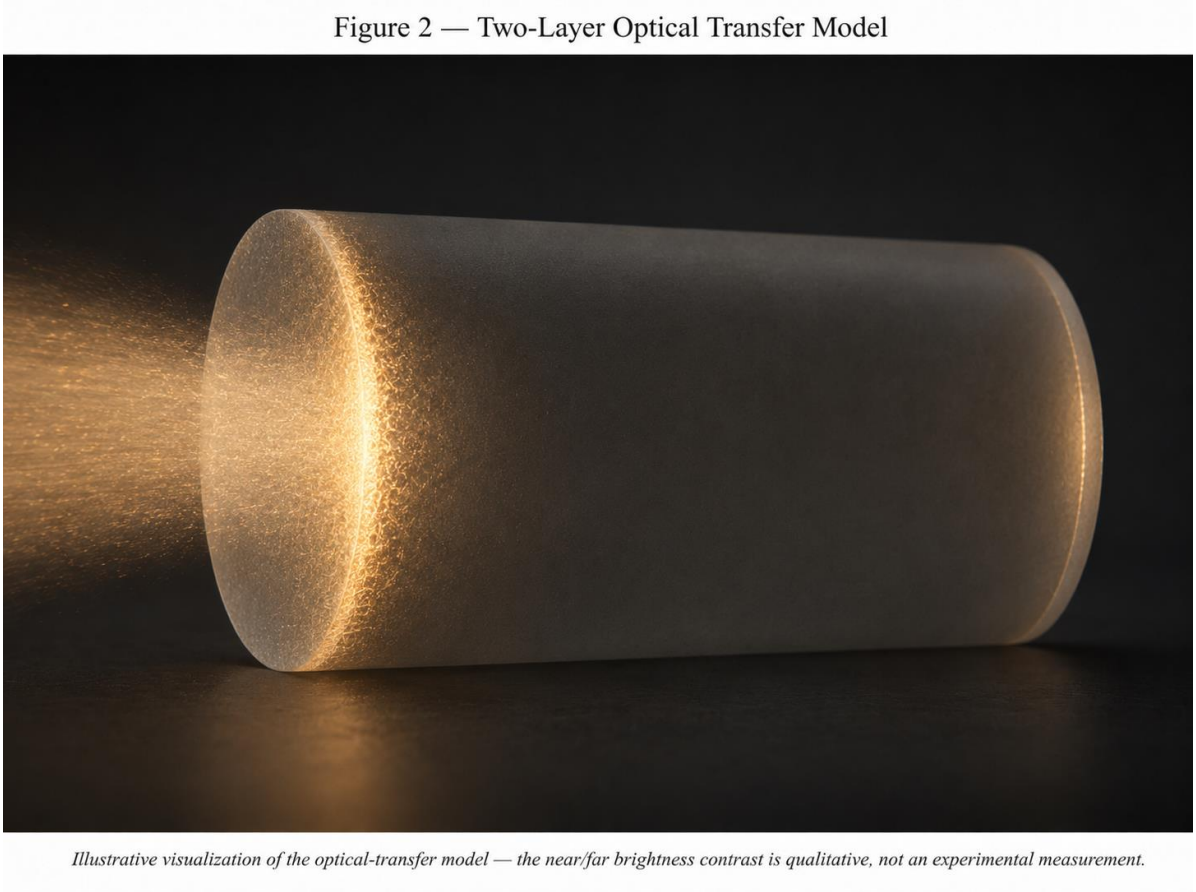


Figure 2. Two-layer optical transfer model (§8.2). Incident light is absorbed and scattered almost entirely within a thin near-side shell (bright glow, left), while the fiber interior remains optically inert and only a faint remnant reaches the far-side shell (right) — illustrating why superficial confinement at both surfaces does not by itself require the two shells to receive comparable absorbed energy. Illustrative visualization; the near/far brightness contrast is qualitative, not an experimental measurement.

8.3 The viable optical escape: combine transfer with a nonlinear chemical response

A directional photon model remains possible if visible coloration is a nonlinear, composition-dependent response rather than a linear map of absorbed dose. A chemically sensitive outer wall could allow both near and far shells to exceed a coloration threshold even when $A_{far} < A_{near}$, while the less reactive interior remains below its own threshold. The required conditions are therefore joint: (i) τ_i must be small enough for substantial transmission through the interior; (ii) the far shell must receive enough energy to cross the outer-layer response threshold; (iii) the interior must remain below its coloration threshold despite transmitted energy; and (iv) the observed near/far color ratio must be reproduced. The decisive quantities are the layer-resolved optical constants

and the response functions of PCW/pectin/coating versus secondary-wall cellulose, not a single transparency number.

Assessment. Directional VUV remains the strongest experimentally demonstrated route to highly superficial photochemical linen coloration [12]. A confirmed circumferential shell would not by itself exclude a photon mechanism, but it would require a quantitatively demonstrated combination of interior transmission and outer-layer chemical selectivity or a secondary circumferential process. This is directly testable (Section 18).

9. Gas-Phase Maillard Reaction

A gaseous mechanism has an immediate geometrical advantage: molecules diffuse around cylindrical fibers, so circumferential access requires no bending of radiation. If Rogers is correct that the reactive carbohydrates form a nanometric external coating (Section 5.3), the same model also yields radial superficiality naturally — the gas permeates pore space, but significant chromophore forms only where the reactive coating exists. Against the 360° observation, this mechanism performs better than often acknowledged.

Its difficulties lie elsewhere, and they are exactly the neighbor-selectivity and longitudinal-switching constraints of Section 6:

- Fiber-to-fiber selectivity. Why would one exposed fiber react strongly while a fiber micrometers away stays clear? Diffusion smooths concentration gradients.
- Longitudinal termination. Why would reaction stop abruptly along a fiber rather than gradually?
- Image resolution. A freely diffusing molecular field broadens gradients over time; a high-resolution image requires very short diffusion distances, strong reaction thresholds, geometry-dependent surface chemistry, or another spatially controlling variable.

Assessment. A Rogers-type gas/coating mechanism is potentially strong for circumferential access, surface-limited chemistry, and low-temperature formation, and weak — without additional physics — for neighbor discrimination, abrupt longitudinal termination, and macroscopic encoding. The unresolved question is not whether gas can color all sides of a fiber (it can) but why it would color only the required fibers and only the required portions of them.

10. Substrate Selectivity: Why Chemical Response ≠ Deposited Energy

The Fanti-PCW and Jaworski-pectin proposals are best understood not as complete image-formation mechanisms but as substrate-selection mechanisms. They answer "why is only the

outside of the fiber chemically vulnerable?" but not "why was this fiber activated and not its neighbor?" They are candidate components of a hybrid, not standalone explanations.

Their key contribution is to break the naive identification of coloration with energy deposition. Chemical response is a nonlinear function

$$response = f(dose, composition, O_2, H_2O, temperature, aging),$$

with, in general, a composition-dependent threshold. If the outer wall has an activation threshold well below the secondary wall's, then even a spatial energy-deposition profile that is nearly uniform across the fiber can produce a color profile that is sharply superficial:

$E_{shell} > E_{th,shell}$ while $E_{int} < E_{th,int}$, even if $E_{shell} \approx E_{int}$.

This distinction is central to the radiation discussion. A dose ratio $S = D_{shell}/D_{int}$ near unity does not logically require a color ratio near unity if the shell and interior have very different precursor concentrations, activation thresholds, quantum yields, oxygen/water dependence, or aging kinetics. Conversely, invoking "chemical sensitivity" cannot be used as a free parameter: the relevant response curves must be measured. The microdosimetry test in Section 22 must therefore be coupled to independently measured dose–response functions rather than judged by dose distribution alone. This decoupling has a limit, however: it rescues a directional model only if the underlying dose asymmetry from Section 8 is modest, not extreme — no plausible chemical-sensitivity difference can equalize a near/far ratio that is already many orders of magnitude apart at the source.

11. Corona Discharge and Electrical Surface Processes

Fanti and collaborators investigated corona discharge because electric fields naturally supply features difficult for optical processes. A dielectric cylinder in a strong field distorts the local field distribution; charges, ions, reactive oxygen species, ozone, local heating, and surface currents need not act only on the illuminated hemisphere. Fanti's work therefore offers corona as a route to superficial and circumferential effects.

Rogers objected on experimental grounds: his plasma/corona exposures produced changes he considered inconsistent with Shroud image fibers, including microscopically visible defects, and he concluded corona/plasma was not involved. Later Fanti work argued that lower-energy corona regimes need not generate the same defects, so the disagreement is partly about which discharge regime is the right comparison. Porter has criticized specific experimental corona images, arguing their coloration distribution does not match the Shroud thread-crown pattern and that the procedure introduced a possible thermal/carbohydrate confound; this is a critique of the

mechanism, not new microscopy establishing the circumferential observation, and it should not be cited as the latter.

Advantages: threshold behavior; circumferential surface effects; preference for exposed regions; stochastic activation. Difficulties: confinement to a submicrometer layer; absence of inappropriate plasma damage; chemical match; abrupt longitudinal transitions; coherent macroscopic intensity. Corona remains physically interesting but experimentally unfinished.

12. Rucker's Two-Stage Radiation/Electrical Model

Robert A. Rucker's Vertically Collimated Radiation Burst (VCRB) hypothesis is relevant because it explicitly separates information transport from fiber coloration. In his January 1, 2026 Paper 44, Rucker proposes an extremely brief vertical oscillation of nuclei in the body; a small fraction of deuterium nuclei are hypothesized to split into protons and neutrons; oscillating protons deposit electrical charge on the cloth and drive alternating current in selected fibers; and the "skin effect" of that current is invoked to confine heating to a thin circumferential outer region. Neutrons are separately invoked to produce additional ^{14}C through $^{14}N(n,p)^{14}C$ [15].

The architecture—directional transport → local activation → circumferential surface chemistry—is conceptually valuable because it decouples the agent that selects image locations from the process that colors a selected fiber. That architecture can be assessed independently of the extraordinary initiating event and independently of whether the specific skin-effect implementation is viable.

12.1 The classical skin-effect implementation is not established for flax

Rucker explicitly applies the classical AC skin-effect concept to flax while acknowledging that a flax fiber is not normally an electrical conductor [15]. The electrodynamic issue is therefore not simply the value of one resistivity. The relevant propagation constant in a linear isotropic medium is

$$\gamma = \sqrt{[\, i\omega\mu\,(\sigma + i\omega\varepsilon)\,]}.$$

In the good-conductor limit, $\sigma \gg \omega\varepsilon$, this reduces to the familiar skin-depth expression $\delta \approx \sqrt{[2/(\omega\mu\sigma)]}$, and current density becomes concentrated near the surface. In the low-loss dielectric limit, $\sigma \ll \omega\varepsilon$, the field is not screened by conduction in the same metallic manner; attenuation and phase propagation are instead controlled by the complex permittivity and dielectric loss. Cellulose and cellulosic materials are ordinarily characterized as dielectrics whose electrical behavior varies strongly with frequency, moisture, temperature, impurities, and structure [19,20]. Therefore the good-conductor skin-depth formula cannot simply be transferred to ordinary flax.

This does not logically exclude every hypothetical transient state of a fiber. It defines the burden of proof. A skin-effect explanation would require a physically specified transient $\sigma(\omega)$, $\varepsilon^*(\omega)$,

temperature, moisture/ionization state, current waveform, and duration for which the fiber enters a regime sufficiently conductive to produce submicrometer radial power confinement, while simultaneously avoiding bulk damage inconsistent with the observed fibers. No such transient material state has yet been measured or quantitatively demonstrated for flax in the proposed context. Experiment 6 (Section 21) is designed to test that requirement.

Assessment. Rucker's two-stage architecture remains a useful conceptual class. His specific AC skin-effect confinement mechanism is presently unsupported for known flax dielectric behavior and should not be treated as demonstrated. A viable electrical version would require either experimentally verified transient conductivity or a different circumferential surface mechanism. The initiating nuclear oscillation itself lies outside established physics; that premise should be kept distinct from the downstream electrodynamic test.

13. A Distinct Gamma/Secondary-Electron Mechanism

A different nuclear mechanism should be considered independently and should not be attributed to Rucker. Thermal neutron capture by ^{14}N through the (n,γ) channel produces ^{15}N and prompt gamma radiation, including a well-established line near 10.83 MeV [18]. At such energies the photon attenuation length in low-Z organic matter is enormously larger than a ~15 μm fiber diameter, so the incident photon field changes negligibly across one fiber. This removes the simple near-side/far-side photon-attenuation asymmetry at the scale of the fiber.

The difficulty then shifts to the charged secondaries. MeV gamma interactions generate Compton electrons and, above the pair-production threshold, electron–positron tracks whose characteristic ranges in low-Z matter are orders of magnitude greater than a 0.2 μm wall [16,17]. The high-energy field therefore tends naturally toward similar average energy deposition at the near and far sides, but not toward confinement of physical dose to an ultrathin shell. Assertions that "secondary electrons are short-range" become relevant only after the energy spectrum and transport of all secondaries are calculated; one cannot replace a MeV-generated spectrum by a preselected keV population without assuming the desired result.

Section 10 prevents this from being an automatic refutation: a relatively broad dose distribution could still produce a sharply surface-limited visible response if the outer layer is chemically far more susceptible than the interior. That possibility makes the coupled problem experimentally sharper, not looser. The transport calculation must predict $D(r,\theta)$, and independent irradiation experiments must determine the response functions of the candidate outer and inner substrates. Only their combination predicts color.

13.1 Coupling of the two nuclear channels

The radiation family can invoke two nitrogen channels: $^{14}N(n,p)^{14}C$ for radiocarbon production and $^{14}N(n,\gamma)^{15}N$ for prompt gamma emission. These yields are coupled through the same neutron spectral fluence rather than through an arbitrary scalar fluence. For channel i, the reaction yield is proportional to $Y_i = N \int \Phi(E)\, \sigma_i(E)\, dE$, where $\Phi(E)$ is the neutron spectral fluence and $\sigma_i(E)$ the energy-dependent cross-section. Therefore any spectrum/fluence chosen to generate a specified gamma field also predicts a corresponding ^{14}C yield, and vice versa. It also predicts activation products in other trace elements. Proposed long-lived products such as ^{36}Cl and ^{41}Ca should be treated as untested side-predictions for targeted measurement, not as presently established absences. The microdosimetry analysis in Section 22 should propagate one common neutron spectrum through all relevant channels as a joint consistency test.

14. The Selectivity-versus-Uniformity Problem, Quantified

A useful conditional result follows for a specific class of stochastic models. Assume (i) neighboring fibers are otherwise comparable in susceptibility, (ii) activation events are independent, (iii) colored-versus-clear selectivity is produced mainly by Poisson variation in the number of qualifying events, and (iv) each event initially affects only a local circumferential patch unless a secondary amplification process occurs. Under these assumptions, rare-event selectivity and smooth circumferential completeness oppose one another.

Let λ_{fiber} be the mean number of qualifying triggers per comparable fiber over the relevant longitudinal segment. If selectivity is generated mainly by event-count fluctuations, appreciable probability for one fiber to remain untriggered while a neighbor is triggered requires λ_{fiber} to be of order unity or smaller:

$$\lambda_{fiber} \lesssim 1. \text{ (selectivity condition)}$$

Now consider circumferential uniformity. Suppose a single qualifying interaction chemically alters only a local patch of the shell subtending a fraction ϕ of the circumference ($\phi < 1$ for a localized electron track or discharge site). To color the full circumference by independent events requires enough interactions in the shell that essentially every angular sector receives at least one:

$$\lambda_{shell} \cdot \varphi \gg 1, \text{ (uniformity condition)}$$

where λ_{shell} is the mean number of qualifying interactions in that fiber's shell over the colored segment. The two λ's are not independent. They arise from the same flux through the same fiber, so λ_{shell} and λ_{fiber} are proportional:

$$\lambda_{shell} = g \cdot \lambda_{fiber},$$

where g = (relevant shell interaction volume)/(fiber cross-section interaction measure) is a geometric factor of order unity or below (the shell is a thin outer fraction of the fiber, so $g \lesssim 1$). Substituting into the uniformity condition:

$$g \cdot \lambda_{fiber} \cdot \varphi \gg 1 \Rightarrow \lambda_{fiber} \gg 1/(g\varphi) \geq 1/\varphi > 1.$$

Under the stated assumptions, these inequalities conflict whenever a single event colors only a small local patch ($\phi \ll 1$). Increasing event density enough to average many independent patches around the circumference also reduces the probability that an otherwise comparable neighboring fiber receives no events. This is not a universal proof against stochastic mechanisms: large fiber-to-fiber variations in coating, chemistry, electric-field enhancement, moisture, or threshold could also create selectivity. It is a conditional demonstration that independent local-hit statistics alone cannot simultaneously be the principal source of neighbor selectivity and a smoothly complete circumferential shell.

The most economical escape within that restricted stochastic class is amplification: one or a few triggers must produce a response over a much larger circumferential domain than the initial interaction patch. Circumferential surface propagation is one such possibility; strong pre-existing fiber heterogeneity is another. Both possibilities are experimentally distinguishable and should be treated as hypotheses rather than assumptions.

15. A Surface-Propagation Hypothesis

The analysis above motivates a two-stage surface-propagation architecture without claiming that it is uniquely required in all models: (1) a directional or otherwise selective event activates a localized region of a fiber; (2) the event creates a radical, charge carrier, thermal excursion, catalytic species, or other trigger; (3) the resulting reaction spreads through a chemically distinct surface layer over a much larger angular domain; and (4) propagation terminates when a local threshold condition ceases to be satisfied.

Schematically: directional/selective trigger → surface initiation → circumferential amplification or propagation. In an independent-event model this separates fiber selection from circumferential coverage; in a heterogeneous-threshold model the same architecture could coexist with local differences in substrate susceptibility.

Candidate propagation processes include radical-chain oxidation; surface charge redistribution; catalytic dehydration; localized ozone chemistry; exothermic reaction within an impurity film; ionic migration through a hydrated PCW; and photochemical excitation migration. None has been demonstrated in ancient flax at the required precision. But the class makes a distinctive, testable prediction at abrupt color boundaries: if coloration propagates circumferentially, the colored-to-clear transition should terminate approximately synchronously around the fiber; if direct

directional exposure dominates, different angular sectors should terminate differently. This is measurable (Experiment 1, Section 16; and Section 25).

PART III — DECISIVE EXPERIMENTS

16. Experiment 1 (Priority): Establish Whether the 360° Shell Exists

This has priority over all mechanism testing. Determine C(r, θ, z) directly on multiple authenticated image fibers, using combinations of confocal Raman microscopy, nano-IR/AFM-IR, synchrotron FTIR, ToF-SIMS chemical mapping, XPS surface analysis, focused-ion-beam serial sectioning, and SEM/TEM of permissible cross-sections, plus hyperspectral or fluorescence-lifetime imaging.

The measurement must resolve: the radial profile (how fast alteration decreases with depth); the circumferential profile (is C(θ) ≈ constant, or is the body-facing hemisphere stronger?); the longitudinal profile (what happens to C at a segment termination — synchronous around the circumference, per Section 15, or sector-dependent?); the chemical identity of the altered layer (structural cellulose, hemicellulose, pectin, or an external carbohydrate coating — resolving Section 5); and replication across multiple fibers, several image intensities, and matched non-image controls. A genuine shell must be shown statistically, not by one representative micrograph.

17. Experiment 2: Quantify Circumferential Completeness

Define an angular coverage index at a stated threshold, $C_f(D_{th}) = (1/2\pi) \int_0^{2\pi} H[D(\theta) - D_{th}]\, d\theta$, with H the step function; $C_f = 1$ is complete coverage, $C_f \approx 0.5$ a hemisphere. Because C_f depends on the (currently unmeasured) threshold, report it as a function of D_{th}, or over a plausible range, rather than as a single number — otherwise it reproduces the false-precision problem this paper criticizes. Report the distribution $p(C_f)$ across fibers (e.g. "80% of image fibers have $C_f > 0.9$ at threshold D_{th}"), and test whether circumferentiality depends on image intensity. Each outcome has distinct mechanistic implications.

18. Experiment 3: Joint Optical-Transfer and Chemical-Response Test of Directional VUV

A decisive transparency experiment must measure more than bulk transmission. On modern flax fibers of Shroud-like diameter, determine wavelength-dependent transmission T(λ), reflection

R(λ), and, where feasible, layer-resolved optical constants for the outer wall and secondary wall from near-UV into VUV. Irradiate individual fibers from one side and chemically map the near shell, interior, and far shell. In parallel, determine dose/fluence–response curves for candidate outer-layer materials (intact PCW, pectin-rich material, Rogers-type carbohydrate coatings) and secondary-wall cellulose. Fit the data with the layered optical model of Section 8, including τs, τi, reflections/scattering where required, and the nonlinear response functions. A single-stage directional model succeeds only if the far external layer reproducibly crosses the Shroud-like coloration threshold, the interior remains below its threshold, and the near/far chemical morphology matches the Shroud measurements. The earlier criterion based on κ = αs/αi alone is insufficient.

19. Experiment 4: Test Gas/Coating Selectivity at Fiber Resolution

Test Rogers's hypothesis for spatial statistics, not merely whether amines yellow linen. Prepare linen under plausible historical processing (generating surface carbohydrate residues); expose to controlled amine concentrations while varying temperature, humidity, exposure time, body-to-cloth spacing, airflow, and surface-carbohydrate concentration; then quantify P(fiber colored | neighbor clear), longitudinal transition length, crown preference, and circumferential coverage. Success requires reproducing the microscopic distribution, not merely producing superficial yellow linen.

20. Experiment 5: Revisit Corona Discharge Without Thermal Confounds

Run untreated linen and chemically characterized coated linen in parallel, varying field strength, waveform, polarity, pulse length, electrode/body geometry, pressure, humidity, ion density, ozone concentration, fiber moisture, and surface conductivity. Analyze exposed fibers with the same pipeline as Shroud image fibers, addressing directly: is coloration circumferential; how deep; are plasma defects present; is it crown-concentrated; can neighbors remain clear; are longitudinal boundaries sharp; does the chemistry fluoresce; does the chromophore match? This adjudicates the Rogers–Fanti disagreement by common method rather than continuing it across incomparable experiments.

21. Experiment 6: Quantitatively Test the Skin-Effect Proposal

Measure complex permittivity and conductivity of single flax fibers or well-characterized flax bundles over the widest experimentally relevant frequency, moisture, temperature, and ionization ranges: σ(ω), ε′(ω), ε″(ω). Then solve Maxwell's equations for a realistic multilayer cylindrical geometry (outer wall, secondary wall, lumen, optional surface coating) using the full

propagation constant $\gamma = \sqrt{[i\omega\mu(\sigma+i\omega\varepsilon)]}$ and compute spatial power deposition. The Rucker skin-effect implementation requires an experimentally defensible transient state in which power deposition is concentrated in a submicrometer circumferential region while the fiber interior remains below the relevant damage/color threshold. Failure to identify such a state would falsify classical skin-effect confinement for the proposed application; discovery of such a state would justify direct pulsed-current experiments.

22. Experiment 7: Microdosimetry Test of the Gamma/Secondary-Electron Model

Construct a Monte Carlo model of one flax fiber plus near-touching neighbors. A representative geometry can use an outer radius $R \approx 7.5$ μm, a thin outer target layer of order 0.2 μm (with sensitivity studies over a wider submicrometer range), a secondary wall, and lumen. Inject photons—not preselected low-energy electrons—using the physically implied prompt-gamma spectrum for $^{14}N(n,\gamma)^{15}N$, with 10.83 MeV included, plus contrast cases at lower photon energies. Use a low-energy coupled photon–electron transport model (e.g., Geant4 Livermore/Penelope, PENELOPE, or MCNP where spatial resolution and production thresholds are demonstrably converged below the target-layer scale). NIST XCOM and ESTAR can provide cross-checks over their validated energy ranges [16,17].

Score dose radially, azimuthally, longitudinally, and in neighboring fibers. Report at minimum: $U = D_{far,outer}/D_{near,outer}$ for circumferential dose symmetry; $S_D = D_{outer}/D_{inner}$ for physical dose superficiality; $Q_D = D_{target}/D_{neighbor}$ for dose selectivity; and the angular sector distribution of deposited energy. Then convert dose to predicted visible alteration using independently measured response functions for the candidate outer and inner substrates. Finally, infer the neutron spectral fluence required to reach the observed coloration and propagate the same $\Phi(E)$ through the $^{14}N(n,p)^{14}C$ and other activation channels. The model is viable only if one physically consistent source spectrum/fluence reproduces the chemical morphology without conflicting radiocarbon or activation-isotope consequences.

23. Comparative Assessment

The table separates how much experimental work exists from how well the mechanism fits the full constraint set, since conflating them (as single "maturity" columns do) is misleading.

MECHANISM	SURFACE CONFINEMENT	360° COMPATIBILITY	NEIGHBOR SELECTIVITY	SHARP LONGITUDINAL SWITCHING	EVIDENCE STATUS
Directional VUV	Strong experimentally	Conditional on layered transfer + chemistry	Possible via threshold/heterogeneity	Possible but not demonstrated	Strong for superficial photochemistry; incomplete morphology
Maillard gas + surface coating	Strong in principle	Natural	Difficult without heterogeneous substrate/thresholds	Difficult under simple diffusion	Chemistry demonstrated; spatial pattern unresolved
PCW / pectin substrate selectivity	Strong	Geometrically natural	Does not by itself explain	Does not by itself explain	Substrate hypothesis, not full transport mechanism
Corona / electrical surface process	Potentially strong	Natural in some regimes	Potentially plausible	Potentially plausible	Contested experiments; incomplete quantitative match
Rucker two-stage architecture	Depends on second stage	Designed to permit	Potentially plausible	Potentially plausible	Conceptual architecture; initiating premise extraordinary
Rucker classical skin-effect implementation	Not established for ordinary flax dielectric regime	Would be circumferential if regime existed	Not sufficient alone	Not sufficient alone	Requires unmeasured transient conductive state
Gamma → secondary electrons	Broad dose; response may still be superficial	Strong for average near/far symmetry	Conditional; rare-hit model conflicts with smooth shell unless amplification/heterogeneity	Problematic alone	Requires coupled transport + chemistry + nuclear-yield test
Surface-amplification / propagation hybrid	Potentially strong	Natural after initiation	Potentially strong	Potentially strong	Conceptual; specific chemistry/electrodynamics not demonstrated

Table 1. Comparative assessment of mechanism classes against the combined microscopic constraint set. "Compatibility" indicates physical plausibility, not historical occurrence.

No mechanism presently reproduces the entire constraint set quantitatively. Two-stage architectures remain especially attractive because they separate spatial selection from local surface chemistry, but no particular second-stage process is established. Likewise, the conditional Poisson result in Section 14 favors amplification only when event-count fluctuations are assumed to be the main source of selectivity among otherwise comparable fibers. Strong substrate heterogeneity remains an alternative that must be measured rather than assumed away.

PART IV — DISCUSSION

24. The Central Paradox Is a Change of Symmetry

If the strong circumferential observation holds, the morphology implies a change of effective symmetry. At cloth scale the image is associated preferentially with body-facing/exposed thread regions; at fiber scale the proposed outer alteration approaches rotational symmetry about the fiber axis. A successful mechanism must therefore explain macroscopic spatial selectivity together with microscopic circumferential response. This is why two-stage architectures deserve particular attention: a directional or otherwise geometry-sensitive information carrier can select locations, while a separate surface process can redistribute or amplify the local chemical response around a selected fiber.

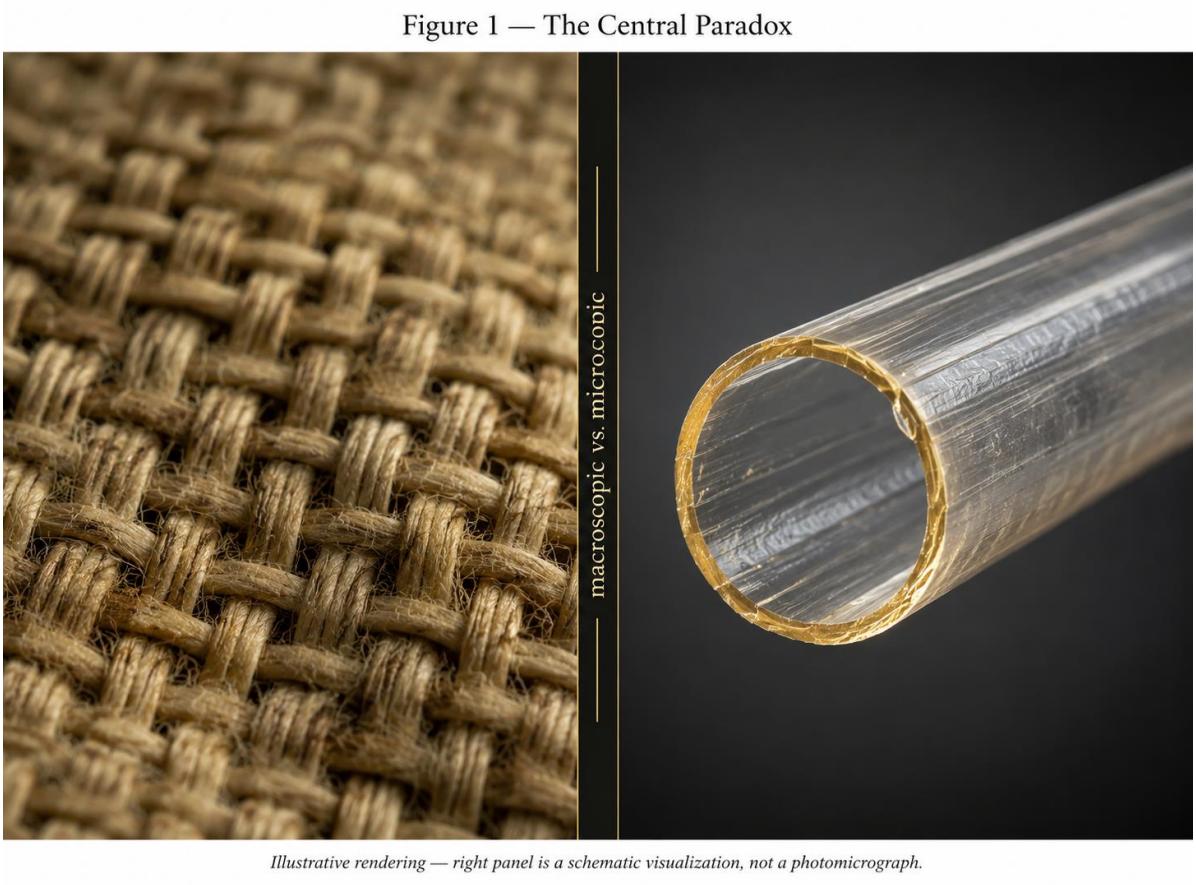


Figure 1. The central paradox (§24). Left: representative linen weave under raking light, illustrating the directional, asymmetric character of the image at cloth and thread scale. Right: schematic visualization of a single fiber cross-section, showing a thin altered shell reported to run the full circumference against a clear interior. The two panels juxtapose opposite symmetries — directional at the macroscopic scale, circumferential at the microscopic scale — that any successful mechanism must reconcile. Illustrative rendering; the right panel is a schematic visualization, not a photomicrograph.

25. What Would Most Strongly Discriminate the Models

The most diagnostic observable may not be average shell thickness but the three-dimensional structure of an abrupt image termination. For a fiber whose color ends at z_0, map the termination around the circumference. Directional exposure predicts the body-facing surface behaves differently from the far surface along z. A diffusing gas predicts a comparatively smooth transition correlated among neighbors. A circumferential electrical threshold predicts several angular sectors switching nearly simultaneously at z_0. Surface-propagating chemistry predicts a propagation front or synchronous circumferential termination. Thus the full $C(r, \theta, z)$ — especially its behavior at terminations — carries far more mechanistic information than any single number such as "0.2 μm."

Figure 5 — Predicted Termination Morphologies

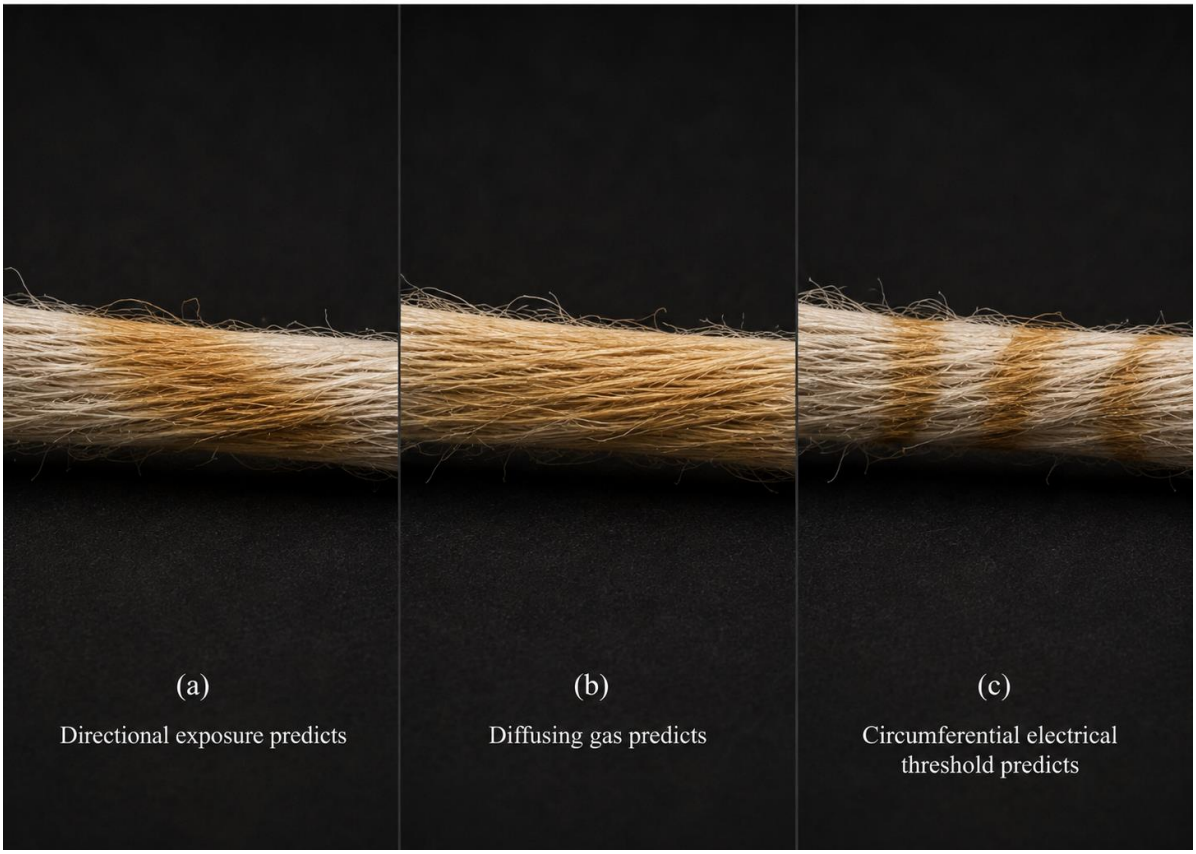


Figure 5. Predicted termination morphologies (§25), the most diagnostic observable proposed in this paper. (a) directional exposure predicts an asymmetric transition, stronger on one side; (b) a diffusing gas predicts a smooth, near-uniform transition around the full circumference; (c) a circumferential electrical threshold predicts a jagged, stepped transition with angular sectors switching at slightly different positions along the fiber. Illustrative rendering, not a photomicrograph of Shroud material.

26. A Necessary Terminological Correction

Discussions should avoid: "STURP proved that every image fiber is colored exactly 0.2 μm deep around all 360°." A defensible formulation is:

STURP established extreme superficiality of the body image at cloth and thread levels and chemical alteration of image fibrils. Later microscopy, particularly the superficiality studies of Fanti and co-workers, reported evidence that the alteration on individual image fibers may occupy an external layer of approximately primary-cell-wall dimensions and extend around the fiber circumference. The reported thickness is on the order of a few tenths of a micrometer, with substantial uncertainty, and the completeness and uniformity of circumferential alteration have not been quantified by modern cross-sectional chemical mapping.

27. Implications if the 360° Shell Is Confirmed

If modern microscopy establishes high circumferential completeness on most image fibers and a far/near chemical ratio close to unity, simple one-stage directional coloration becomes difficult. A directional optical model would survive only if the measured layered optical transfer and nonlinear response curves quantitatively reproduce both sides while sparing the interior, or if a secondary circumferential process is present. Pure surface-contact models would likewise face a severe geometric constraint. The most plausible remaining classes would include isotropic local agents, electrical redistribution under a demonstrable material regime, and triggered surface amplification/propagation.

28. Implications if the 360° Shell Is Not Confirmed

If mapping finds $C_{near} > C_{far}$ with only partial or variable circumferential alteration, that is equally important: it would mean the strong 360° constraint arose from optical interpretation of a limited fiber sample rather than a universal morphology, and directional VUV, proton, electron, or other radiation mechanisms would become substantially easier to reconcile with the fiber data. The value of the measurement does not depend on its outcome; either result sharply reduces the hypothesis space.

29. Limitations and Critical Perspectives

29.1 Source concentration and independence

This paper evaluates candidate mechanisms for circumferential coloration largely within a specific research literature — STURP-derived analyses, the Fanti/Padua group, Rogers, Jaworski, Porter, and Rucker — most of it published through Shroud-focused conferences, Shroud.com, the Shroud Research Network, and specialty venues such as the International Journal of Archaeology, rather than through the broader materials-science, analytical-chemistry, or nuclear-physics literature with independent peer review. That concentration is not itself disqualifying — a narrow

empirical question can have a narrow literature — but it means the evidentiary base for the strong circumferential claim rests on a small, non-independent cluster of studies rather than replicated, cross-laboratory confirmation. The ~0.2 ± 0.2 μm estimate central to Sections 3 and 6, for example, traces to a single optical measurement by one research group at one lacuna on one tape-extracted fiber [6], and has not been independently reproduced with modern nanoscale chemical imaging in the fifteen years since. The mechanism comparisons in Part II should be read with this in mind: they weigh hypotheses against a constraint set that is itself less secure than its central role in this paper might suggest.

29.2 A convergence that should raise suspicion, not confidence

Section 12 treats Rucker's Vertically Collimated Radiation Burst hypothesis as a candidate mechanism for circumferential coloration, evaluated there on its electrodynamic merits. What that treatment does not foreground is that the same hypothesis, in the same source, is also explicitly offered to reconcile the image with the 1988 radiocarbon date — the title of Rucker's Paper 44 is "Hypothesis to Explain the Image Formation and Carbon Dating on the Shroud of Turin" [15]. A single, unreplicated, and physically unestablished mechanism — a hypothesized brief vertical nuclear oscillation, invoking a material state never observed — is thereby asked to simultaneously solve two independent problems: how the image formed, and why an otherwise well-replicated radiometric date disagrees with the traditional dating of the object. That two unrelated puzzles would happen to share one solution is logically possible, but it is exactly the kind of coincidence that should lower rather than raise confidence in the mechanism, absent independent evidence for the underlying event. Treating the neutron-irradiation component as a source of additional ^{14}C (Sections 12–13.1) without independently establishing that the irradiation itself occurred argues from the conclusion: the irradiation is motivated by the need to explain the date, not by independent physical evidence that it happened.

29.3 The radiocarbon date deserves primary, not incidental, treatment

The 1988 radiocarbon dating of the Shroud remains the most direct, replicated, and methodologically independent physical measurement of the cloth's age: three accelerator mass spectrometry laboratories (Oxford, Zurich, and Arizona), working independently, dated the linen to 1260–1390 CE with better than 95% confidence [21]. This is a different evidentiary category from the circumferential-coloration literature discussed above: it is a quantitative, cross-laboratory-replicated measurement of the object itself, not an optical interpretation of a single image fiber. A paper that devotes more than twenty sections to physical mechanisms for image formation and addresses the radiocarbon date only in a few sentences embedded inside a discussion of Rucker's neutron hypothesis has allocated its scrutiny asymmetrically. That imbalance matters: a paper can be rigorous section by section and still read, in aggregate, as a brief for one conclusion rather than

a balanced inquiry if its scrutiny is distributed unevenly across the evidence that supports that conclusion and the evidence that complicates it.

None of the mechanisms evaluated in Part II, including a confirmed 360° circumferential shell, would by itself overturn or explain the radiocarbon result; conversely, no image-formation mechanism proposed here requires the cloth to be of any particular age. The two questions — how did the image form, and when was the cloth woven — are logically separable, and this paper's scope (Section 1) is explicitly the former. But separable is not the same as unrelated in the reader's assessment of the whole, and a paper on Shroud image physics that engages carbon dating only through a single reconciliation hypothesis, without citing the original dating study or the substantial literature defending it against contamination and repair-patch objections, risks leaving the impression that the radiocarbon question has been addressed when it has only been gestured at.

These limitations do not invalidate the physical analysis in Parts I–III, which stands on its own for the narrower question of whether specific proposed mechanisms are consistent with the reported microscopic evidence. They do mean that this paper should be read as one contribution within a contested literature rather than a neutral survey of it, and that the radiocarbon evidence in particular should be weighed independently, and with at least the same rigor applied here to circumferential coloration.

30. Conclusion

Circumferential coloration occupies an unusual position in Shroud image literature: it is potentially one of the strongest physical constraints on image formation, yet it is less comprehensively measured than the cloth- and thread-level superficiality with which it is often bundled. STURP-era work strongly supports an image concentrated on exposed cloth/thread surfaces, lack of liquid capillary penetration, and chemical alteration of image fibrils rather than sufficient applied pigment to account for the body image [1–4]. Later microscopy, principally Fanti et al. [6], provides substantive evidence that the alteration on examined image fibers occupies an external submicrometer region and may extend circumferentially. Their ~0.2 ± 0.2 μm estimate is important but should not be treated as an exact universal shell thickness.

The central problem is the conjunction of constraints: radial superficiality, thread-crown preference, neighboring colored and clear fibers, abrupt longitudinal termination, possible circumferential completeness, and coherent macroscopic encoding. No proposed mechanism reproduces the whole set quantitatively. Directional VUV demonstrates that highly superficial flax photochemistry is experimentally possible, but a confirmed 360° shell would require a joint optical-transfer and chemical-response solution rather than a simple transparency claim. A Rogers-type gas/coating model naturally permits circumferential superficial chemistry but has

difficulty with microscopic selectivity and sharp switching. Corona/electrical mechanisms provide plausible threshold and circumferential behavior but remain experimentally incomplete. Rucker's two-stage architecture is conceptually relevant, whereas his specific classical skin-effect implementation requires a transient conductive state not yet demonstrated for flax. The independent gamma/secondary-electron model removes the simple near/far photon asymmetry but must survive coupled microdosimetry, chemistry, and nuclear-yield tests.

The highest priority is therefore to measure $C(r,\theta,z)$ directly on multiple authenticated image fibers with modern surface-sensitive methods: radial depth, angular completeness, longitudinal termination morphology, and chemical composition. If a continuous ultrathin circumferential shell is confirmed, the result will severely constrain one-stage directional mechanisms and make some form of surface-selective amplification, redistribution, or isotropic local chemistry increasingly attractive. If it is not confirmed, one of the strongest objections to directional models substantially weakens. Either result would be genuine progress, making this one of the most discriminating microscopic measurements available for future Shroud research.

Source-Critical and Methodological Note

Two points require explicit source discipline. First, Adler's statement that image fibers are "uniformly colored" is immediately explained by him as an areal-density or halftone observation—an exposed fiber is colored or not colored—and should not by itself be cited as a direct 360° cross-sectional measurement [4]. The stronger cylindrical-surface formulation appears explicitly in the 2005 Shroud Science Group catalogue [5] and is argued observationally by Fanti et al. [6].

Second, the ~0.2 μm figure is not merely an experimental-laser surrogate. Fanti et al. describe a lacuna in the outer layer of a tape-extracted Shroud image fiber and report an optical estimate of approximately 0.2 ± 0.2 μm [6]. The limitation is therefore not absence of a Shroud-fiber observation but its precision, representativeness, and methodology. The field still lacks a replicated nanoscale chemical map showing shell thickness and chemical composition as a function of angle and longitudinal position across a statistically useful set of authenticated image fibers.

Finally, the present paper intentionally distinguishes directly observed Shroud properties, proposed substrate identifications, experimentally reproduced analogues, and speculative initiating mechanisms. The ranking of mechanisms is therefore conditional on the strong circumferential premise and should be revised if modern fiber mapping changes that premise.

AI-Assistance Disclosure

This manuscript was written with the support and assistance of AI tools for literature organization, language refinement, comparative structuring, and formulation of testable physical arguments. The author reviewed the manuscript and assumes responsibility for the scientific claims, interpretations, citations, and conclusions presented here.

Conflict of Interest

The author declares no competing financial interest relevant to this manuscript.

References

Schwalbe, L. A., & Rogers, R. N. (1982). Physics and chemistry of the Shroud of Turin: A summary of the 1978 investigation. Analytica Chimica Acta, 135, 3–49. https://doi.org/10.1016/S0003-2670(01)85263-6

Heller, J. H., & Adler, A. D. (1981). A chemical investigation of the Shroud of Turin. Canadian Society of Forensic Science Journal, 14(3), 81–103. https://doi.org/10.1080/00085030.1981.10756882

Jumper, E. J., Adler, A. D., Jackson, J. P., Pellicori, S. F., Heller, J. H., & Druzik, J. R. (1984). A comprehensive examination of the various stains and images on the Shroud of Turin. In Archaeological Chemistry III, ACS Advances in Chemistry Series 205, 447–476. https://doi.org/10.1021/ba-1984-0205.ch022

Adler, A. D. (1999). The nature of the body images on the Shroud of Turin. Proceedings of the Shroud of Turin International Research Conference, Richmond, Virginia. Available from Shroud.com.

Fanti, G., Schwortz, B., Accetta, A., Botella, J. A., Buenaobra, B. J., Carreira, M., et al. (2005). Evidences for testing hypotheses about the body image formation of the Turin Shroud. Third Dallas International Conference on the Shroud of Turin, Dallas, Texas, September 8–11, 2005.

Fanti, G., Botella, J. A., Di Lazzaro, P., Heimburger, T., Schneider, R., & Svensson, N. (2010). Microscopic and macroscopic characteristics of the Shroud of Turin image superficiality. Journal of Imaging Science and Technology, 54(4), 040201-1–040201-8. https://doi.org/10.2352/J.ImagingSci.Technol.2010.54.4.040201

Moran, K., & Fanti, G. (2002). Does the Shroud body image show any physical evidence of Resurrection? IV Symposium Scientifique International du CIELT, Paris, April 25–26, 2002.

Rogers, R. N., & Arnoldi, A. (2003). The Shroud of Turin: An amino-carbonyl reaction (Maillard reaction) may explain the image formation. Melanoidins, 4, 106–113. Office for Official Publications of the European Communities, Luxembourg.

Rogers, R. N. (2005). The Shroud of Turin: Radiation effects, aging and image formation. Online technical paper, Shroud.com.

Fanti, G. (2010). Can a corona discharge explain the body image of the Turin Shroud? Journal of Imaging Science and Technology, 54(2), 020508-1–020508-11. https://doi.org/10.2352/J.ImagingSci.Technol.2010.54.2.020508

Fanti, G., Lattarulo, F., & Scheuermann, O. (2005). Body image formation hypotheses based on corona discharge. Third Dallas International Conference on the Shroud of Turin, Dallas, Texas, September 8–11, 2005.

Di Lazzaro, P., Murra, D., Nichelatti, E., Santoni, A., & Baldacchini, G. (2012). Superficial and Shroud-like coloration of linen by short laser pulses in the vacuum ultraviolet. Applied Optics, 51(36), 8567–8578. https://doi.org/10.1364/AO.51.008567

Jaworski, J. S. (2025). The role of pectins in the body image formation on the Turin Shroud. International Journal of Archaeology, 13(2), 178–184. https://doi.org/10.11648/j.ija.20251302.15

Porter, J. C. (2026). The Shroud of Turin's improbable body image. International Journal of Archaeology, 14(1), 1–4. https://doi.org/10.11648/j.ija.20261401.11

Rucker, R. A. (2026). Hypothesis to Explain the Image Formation and Carbon Dating on the Shroud of Turin. Shroud Research Network, Paper 44, January 1, 2026.

Berger, M. J., Coursey, J. S., Zucker, M. A., & Chang, J. (2005). ESTAR, PSTAR, and ASTAR: Computer programs for calculating stopping-power and range tables for electrons, protons, and helium ions (Version 1.2.3). National Institute of Standards and Technology, Gaithersburg, MD.

Berger, M. J., Hubbell, J. H., Seltzer, S. M., Chang, J., Coursey, J. S., Sukumar, R., Zucker, D. S., & Olsen, K. (2010). XCOM: Photon Cross Section Database (Version 1.5). National Institute of Standards and Technology, Gaithersburg, MD.

Rose, P. B., Jr., & Erickson, A. S. (2018). High-energy γ rays resulting from low-energy nuclear reactions in light nuclei. Physical Review C, 97, 064305. https://doi.org/10.1103/PhysRevC.97.064305

Jackson, J. D. (1998). Classical Electrodynamics (3rd ed.). Wiley, New York.

Luo, Q., Shen, H., Zhou, G., & Xu, X. (2023). A mini-review on the dielectric properties of cellulose and nanocellulose-based materials as electronic components. Carbohydrate Polymers, 303, 120449. https://doi.org/10.1016/j.carbpol.2022.120449

Damon, P. E., Donahue, D. J., Gore, B. H., Hatheway, A. L., Jull, A. J. T., Linick, T. W., et al. (1989). Radiocarbon dating of the Shroud of Turin. Nature, 337, 611–615. https://doi.org/10.1038/337611a0